

Article

Facile Green Preparation of Rhodium Nanoclusters Supported Nano-Scaled Graphene Platelets for Sonogashira Coupling Reaction and Reduction of p-Nitrophenol

Gopiraman Mayakrishnan ¹, Saravanamoorthy Somasundaram ², Sana Ullah ³,
Ilangoan Andivelu ², Kim Ick Soo ^{3,*} and Chung Ill Min ^{1,*}

¹ Department of Crop Science, College of Sanghur Life Science, Konkuk University, Seoul 05029, Korea.; gopiramannitt@gmail.com

² School of Chemistry, Bharathidasan University, Tiruchirappalli, Tamil Nadu 620-024, India; saraartudc@gmail.com (S.S.); ilangoan@bdu.ac.in (I.A.)

³ Nano Fusion Technology Research Group, Division of Frontier Fibers, Institute for Fiber Engineering (IFES), Interdisciplinary Cluster for Cutting Edge Research (ICCER), Shinshu University, Tokida 3-15-1, Ueda, Nagano Prefecture 386-8567, Japan; sanamalik269@gmail.com

* Correspondence: kimicksoo.gr@gmail.com (K.I.S.); illminchung@gmail.com (C.I.M.); Tel.: +82-02-450-3730 (C.I.M.); Fax: +82-02-446-7856 (C.I.M.)

Received: 27 September 2019; Accepted: 23 October 2019; Published: 30 October 2019



Abstract: Rhodium nanoclusters were uniformly dispersed on nano-scaled graphene platelets by a simple ‘mix and heat’ method without using any toxic reagents. Distilled water was used to obtain the homogenous dispersion of Rh-nanoclusters on graphene platelets. The morphology of the resultant catalyst (Rh(0)NCs/GNPs) was studied by means of transmission electron microscope (TEM) and atomic force microscope (AFM) analyses. The X-ray photoemission spectroscopy (XPS) result confirmed the metallic form of Rh-nanoclusters in Rh(0)NCs/GNPs. The crystalline property and the interaction between Rh-nanoclusters and graphene platelets (GNPs) were studied by means of XRD and Raman analysis. The Rh-loading in Rh(0)NCs/GNPs was confirmed by scanning electron microscope and energy dispersive spectroscopy (SEM-EDS) and inductively coupled plasma-mass spectroscopy (ICP-MS) analysis. After being optimized, the Rh(0)NCs/GNPs used as catalyst for the reduction of 4-nitrophenol with NaBH₄ and the Sonogashira coupling reaction between iodobenzene with phenylacetylene. To our delight, the Rh(0)NCs/GNPs showed excellent catalytic activity towards the reduction of 4-nitrophenol with an excellent turnover frequency (TOF) value of 112.5 min⁻¹. The k_{app} and k' values were calculated to be $62.07 \times 10^{-3} \text{ min}^{-1}$ (0.002 mg of Rh(0)NCs/GNPs) and $31035 \times 10^{-3} \text{ mg}^{-1} \text{ min}^{-1}$, respectively. Alike, under the optimal conditions, the Rh(0)NCs/GNPs gave the desired product, diphenylacetylene, in a good yield of 87% with 91% selectivity. The Rh(0)NCs/GNPs can be reused without significant loss in its catalytic activity.

Keywords: grapheneplatelets; Rh-nanoclusters; green preparation; 4-Nitrophenol; C–C coupling reaction; reusability

1. Introduction

Transition metal nanoparticles, such as Ru, Rh, and Pd, are often found to be efficient catalysts for a wide range of organic reactions, including hydrogenation of unsaturated compounds and reductive coupling of aryl halides [1,2]. In particular, Rh-nanoparticles are known for their very high catalytic activity in hydrocarbonylation, hydrogenation, hydroformylation, and reductive coupling reactions [3].

Most of the findings show that the activity of Rh-nanoparticles is size and shape dependent. To date, a considerable number of Rh-nanostructures with various sizes and shapes are developed [4,5]. Zhang and co-workers [6] recently reported slow-injection polyol methods for the preparation of size-tunable Rh nanostructures. They tuned the size of Rh-nanostructures (with edge lengths of 15–59 nm) by simply varying the concentration of Rh precursors. Similarly, Kang et al. [7] demonstrated morphology-controlled preparation of Rh-nanoparticles for cancer phototherapy. In spite of that, the Rh-nanostructures are less studied in the catalytic organic transformations due to low stability, poor reusability, and high cost. Various support materials, such as porous carbon, silica, and alumina, are used to stabilize the Rh-nanostructures to overcome the drawbacks. For instance, Siebels et al., [8] employed Rh-nanoparticles supported triazine-based frameworks as catalyst (Rh@CTF-1 composite) for benzene hydrogenation and hydrogen evolution reaction. They found that the Rh@CTF-1 composite is highly stable and reusable. Motoyama et al. [9] used carbon nanofibers (CNFs) as support for the immobilization of Rh-nanoparticles and the resultant Rh-catalyst (Rh/CNF-T) was used for arene hydrogenation. Surprisingly, the Rh/CNF-T was found to be highly activity, even under mild reaction conditions and the catalyst obtained very high TON values. More importantly, no leaching of Rh-species was found during the catalytic reaction. In spite of the remarkable catalytic activity, very a limited number of carbon supported Rh-nanocatalyst being reported for the organic transformation to date. Hence, the development of highly active, reusable, and stable supported-Rh-catalyst, particularly, for organic reaction, deserves special attention.

Recently, nano-scaled graphene platelets (GNPs) are found to be a highly suitable platform for the decoration of catalytic metal nanoparticles [10–13]. The GNPs-supported metal nanoparticles demonstrated superior catalytic activity in various organic reactions [14]. Particularly, the GNPs-supported catalysts that were prepared via dry synthesis ('mix and heat' method) played a remarkable role in heterogeneous catalysis. In fact, the preparation method not only provides good metal-support interaction, but also produces additional defect sites [15]. Moreover, the preparation method is green and uses no toxic reducing or stabilizing agents. For example, an inactive RuO₂-catalyst was activated by decorating it on single-walled carbon nanotubes via the 'mix and heat' method for Heck coupling reaction [16]. They found that the resultant catalyst (RuO₂/SWCNT) is highly active, stable, and reusable. Similarly, various nanocatalysts, such as CuO/GNS [17], RuO₂/MWCNTs [18], CuO/MWCNTs [19], Ru/GNSs [20], Ni/GO [21], NiO/CNP [22], RuO₂NPs/GNPs [23], and CuO/CNP [24], were prepared and efficiently employed for the organic transformations. Hence, we believe that the simple decoration of Rh-nanoclusters on nano-scaled graphene platelets would give an efficient, stable, and reusable nanocatalyst for organic conversions, such as a reduction of 4-nitrophenol and Sonogashira coupling reaction. In fact, the catalytic conversion of hazardous 4-nitrophenol to valuable 4-aminophenol is a highly significant process in green chemistry [24]. Similarly, the transition metal catalyzed Sonogashira coupling reaction between terminal alkynes and aryl halides is a significant tool in organic synthesis [25]. The catalytic products can be used in pharmaceuticals and fine chemicals. To the best of our knowledge, there is no efficient and stable Rh-based graphene catalyst reported for the reduction of nitrophenols and Sonogashira cross coupling reaction. Herein, we prepared Rh(0)-nanoclusters supported nano-scaled graphene platelets (Rh(0)NCs/GNPs) by a simple 'mix and heat' method. Green solvent, water, was used for the homogeneous decoration of Rh(0)-nanoclusters on GNPs. The Rh(0)NCs/GNPs was characterized by transmission electron microscope (TEM), atomic force microscope (AFM), scanning electron microscope and energy dispersive spectroscope (SEM-EDS), inductively coupled plasma-mass spectroscope (ICP-MS), Raman, X-ray diffraction (XRD), and X-ray photoemission spectroscope (XPS) analysis. After being characterized, the Rh(0)NCs/GNPs was used for the reduction of 4-nitrophenol and Sonogashira coupling reaction. The reusability and stability of the Rh(0)NCs/GNPs were also studied.

2. Results and Discussion

2.1. Characterization of Rh(0)NCs/GNPs Catalyst

Toxic reducing or stabilizing agents free simple ‘mix and heat’ method was adopted for the preparation of Rh(0)NCs/GNPs. Distilled water was used as solvent for achieving uniform mixing of GNPs and Rh(acac)₃. Finally, the calcination of GNPs/Rh(acac)₃ mixture under inter atmosphere obtained the homogenous dispersion of Rh(0)NCs on nano-scaled graphene platelets. The purpose of this simple preparation is to achieve big size of Rh nanoclusters (between 25–100 nm) on the surface of GNPs. In fact, the high surface energy of small Rh-nanoparticles (0.1–10 nm) would be expected to favor “Rh leaching-catalytic reaction-Rh readsorption” mechanism and dissolution tendency of small Rh-nanoparticles. According to Kanuru et al. [26], the bulky molecules (reactants) can easily accommodate on the big-size Rh-nanoparticles, whereas, in the case of small Rh-nanoparticles, molecular decomposition is possible due to the bond breaking of molecules adsorbed on the surface of Rh-nanoparticles. In addition, they noticed that the catalytic activity of the Rh-catalyst is mainly due to differences in particle size rather than particle morphology. Alike, Yuan et al. [27] found that the small size of Rh-nanoparticles (under ~10 nm) is more prone towards self-oxidation, which results in catalytically inactivity or promoting side reactions. We presumed that the present Rh-nanoclusters with an average size of 72 nm supported on GNPs could be highly suitable for the catalytic applications.

Figure 1 depicts the TEM images of fresh GNPs and Rh(0)NCs/GNPs catalyst. Figure 1 shows the size distribution of Rh-nanoclusters in Rh(0)NCs/GNPs. It can be seen that the fresh GNPs showed two-dimensional (2D)-sheet like morphology (with thickness of ~39 nm) without any impurities. The TEM images of Rh(0)NCs/GNPs confirmed that the Rh-nanoclusters with an average size of ~72 nm were strongly attached on the surface of GNPs. The high resolution TEM image of Rh(0)NCs/GNPs (Figure 1e) reveal that the big-size of Rh-nanoclusters are accumulated by very fine Rh-nanoparticles. Figure 1 shows the size distribution of Rh-nanoclusters in Rh(0)NCs/GNPs and the mean size of Rh-nanoclusters is found to be ~72 nm and the standard deviation was calculated to be ~30 nm. To further one-dimensional (1D) and three-dimensional (3D) AFM profiles of fresh GNPs and Rh(0)NCs/GNPs were also captured (Figure 2). The AFM profile of fresh GNPs showed smooth and sheet-like surface morphology without the presence of Rh-nanoclusters. However, the 1D and 3D AFM profiles of Rh(0)NCs/GNPs demonstrate rough surface morphology with the uniform decoration of Rh-nanoclusters. The Rh-nanoclusters size of about 75 nm was calculated from the AFM profiles, which agrees well with the TEM results. The mean roughness (Rq) values were obtained for fresh GNPs and Rh(0)NCs/GNPs. The Rq values of 86 and 23 nm were calculated for fresh GNPs and Rh(0)NCs/GNPs, respectively. The significant decrease in the Rq value for Rh(0)NCs/GNPs when compared to fresh GNPs proves the successful decoration of Rh-nanoclusters.

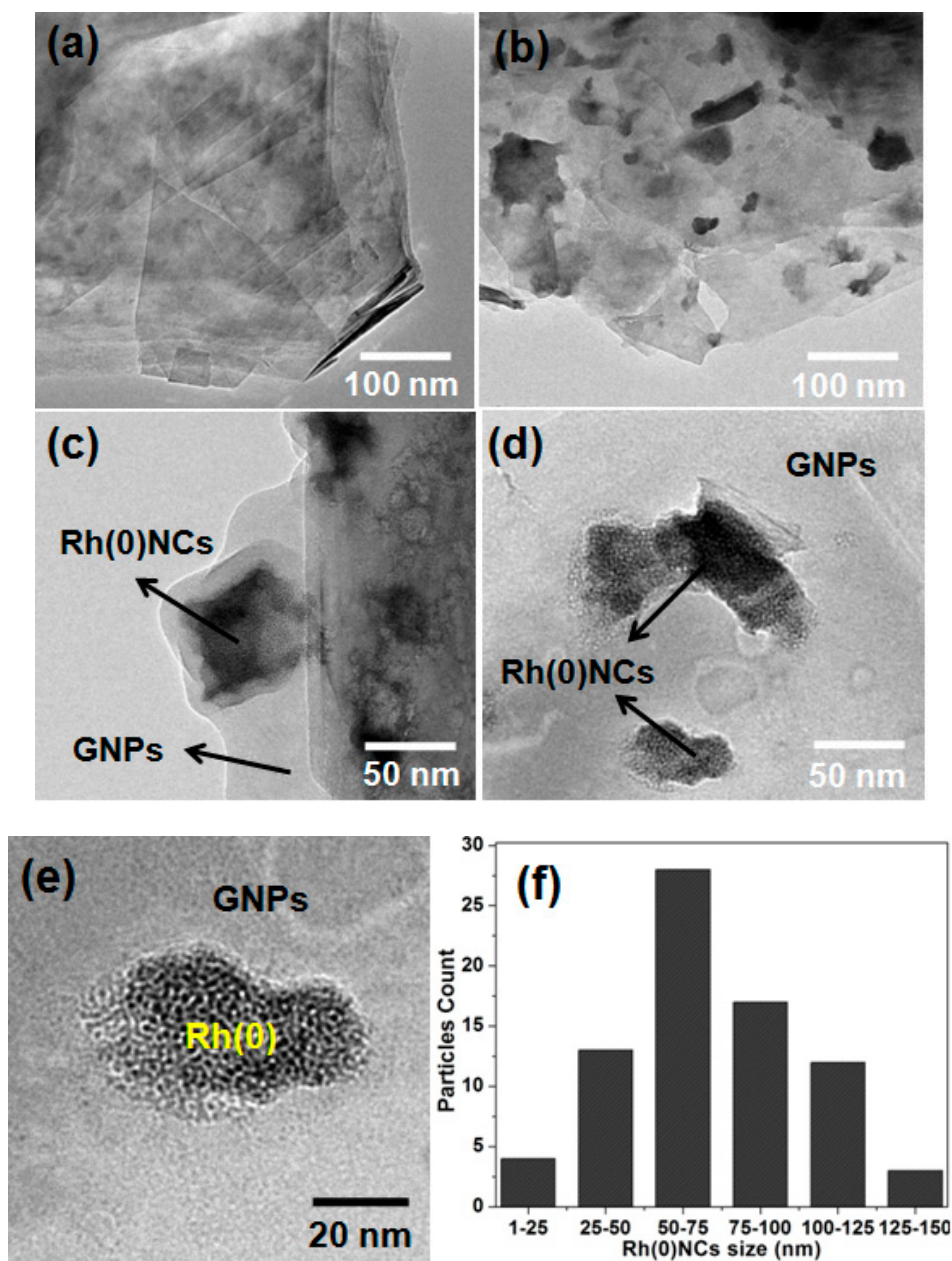


Figure 1. Transmission electron microscope (TEM) images of (a) fresh GNPs, (b–e) Rh(0)NCs/GNPs, and (f) the size distribution of Rh-clusters in Rh(0)NCs/GNPs.

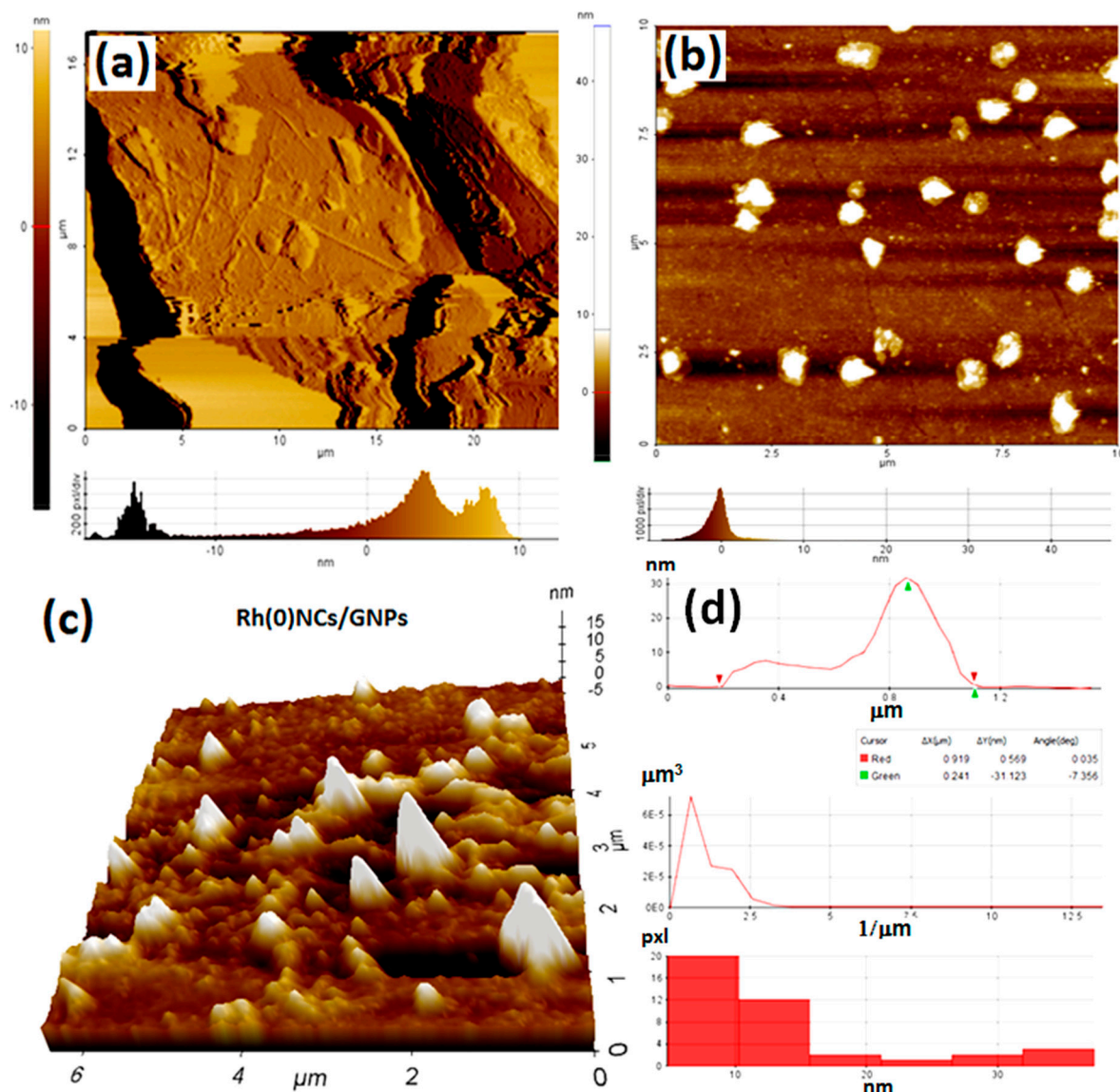


Figure 2. Atomic force microscope (AFM) one-dimensional (1D) and three-dimensional (3D) profile of (a) graphene platelets (GNPs) and (b,c) Rh(0)NCs/GNPs and (d) the particle size distribution of Rh nanoparticles in Rh(0)NCs/GNPs.

The Rh-content in Rh(0)NCs/GNPs catalyst was determined by means of SEM-EDS analysis. Figure 3 shows the SEM image and EDS spectrum of Rh(0)NCs/GNPs, and the corresponding elemental mapping of C, O, and Rh. It was found that the Rh(0)NCs/GNPs only contains C, O, and Rh elements, indicating that the present Rh(0)NCs/GNPs is highly pure and free from any impurities. The factual content of C, O, and Rh was determined to be 83.78, 12.57, and 3.65 wt%, respectively. Moreover, the elemental mapping of C, O, and Rh demonstrates the homogenous dispersion of Rh-nanoclusters on the surface of GNPs.

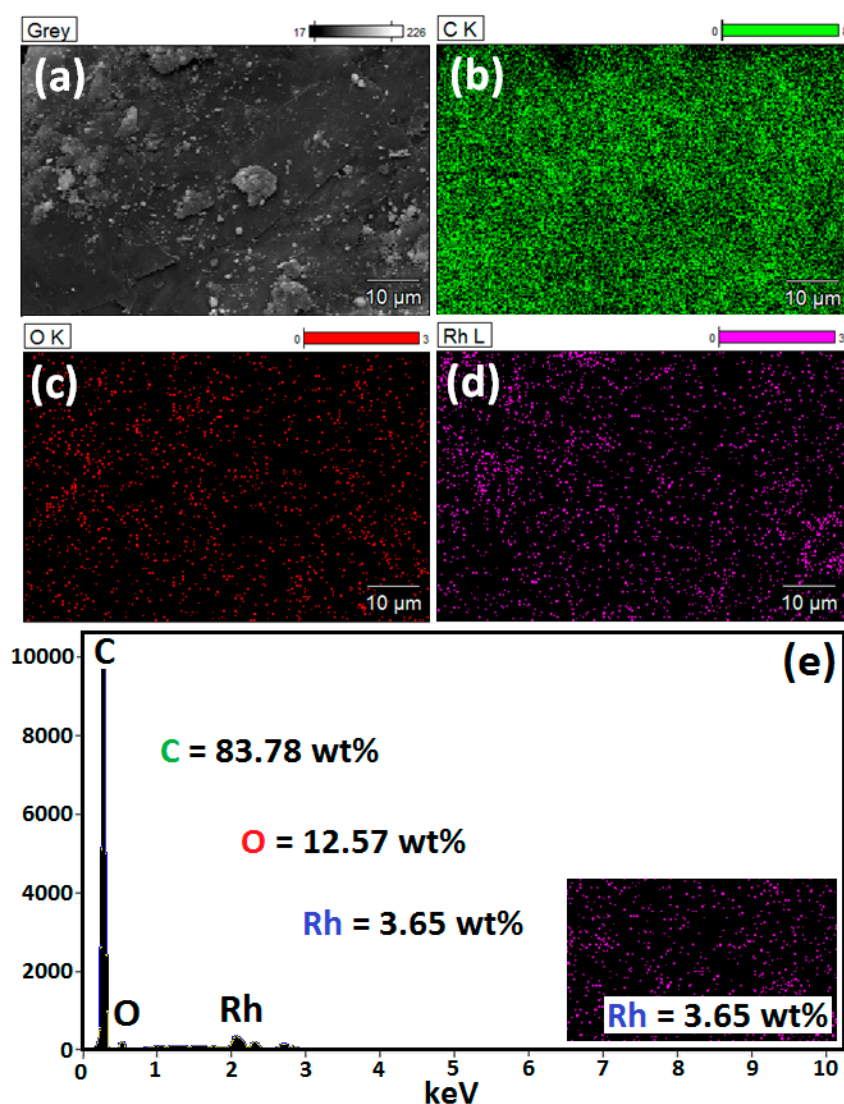


Figure 3. (a) Scanning electron microscope (SEM) image of Rh(0)NCs/GNPs and corresponding (e) energy dispersive spectroscopy (EDS) spectrum and elemental mapping of (b) C, (c) O, and (d) Rh.

Raman spectra were recorded for fresh GNPs and the Rh(0)NCs/GNPs catalyst. Three characteristic peaks were noticed, D band at $\sim 1350\text{ cm}^{-1}$, G band at $\sim 1590\text{ cm}^{-1}$ and 2D band at $\sim 2730\text{ cm}^{-1}$, for both fresh GNPs and Rh(0)NCs/GNPs (Figure 4). The presence of most intense G band refers to in-plane/out-of-plane vibrational modes of sp^2 hybridized carbon orbitals [28]. The D band at 1350 cm^{-1} (disorder induced) indicates that the defects are present in the GNPs [29]. In addition, the 2D band at $\sim 2730\text{ cm}^{-1}$ is attributed to overtone of D band and D + G band [28]. The 2D peak reflects the stacking structure of graphite along the c-axis. The I_D/I_G and I_{2D}/I_G ratios were calculated for the GNPs and Rh(0)NCs/GNPs catalyst (Figure 4). The I_D/I_G ratio of 0.071 ± 0.012 and 0.112 ± 0.012 was calculated for GNPs and Rh(0)NCs/GNPs, respectively. Similarly, the I_{2D}/I_G ratio of GNPs and Rh(0)NCs/GNPs was calculated to be 0.426 and 0.461, respectively. The significant increase in the I_D/I_G and I_{2D}/I_G ratios of Rh(0)NCs/GNPs when compared to GNPs shows that the Rh(0)NCs/GNPs has more defects than that of GNPs. The increase in the defect sites is mainly due to the decoration of Rh-nanoclusters on the surface of GNPs [30]. In addition, the mechanical exfoliation of GNPs (during the ‘mix and heat’ preparation of Rh(0)NCs/GNPs) might also be the reason for the relatively high defects present in the Rh(0)NCs/GNPs catalyst. The 2D band intensity of Rh(0)NCs/GNPs is seen to be high when compared to the GNPs, which also conform the mechanical exfoliation or an increase in the amorphous fraction of GNPs during the preparation process [29].

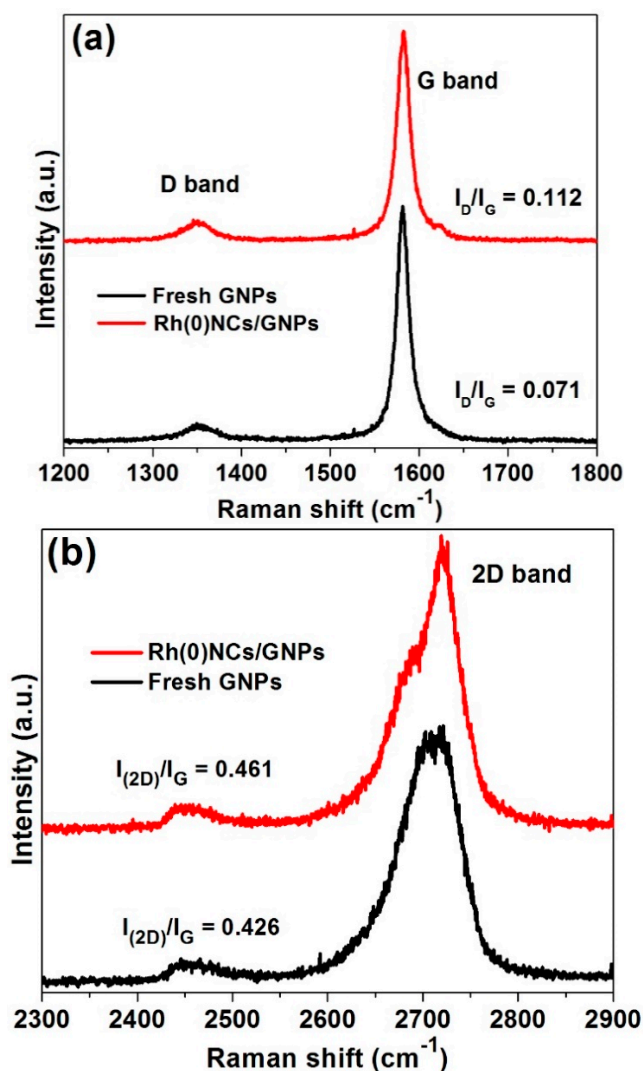


Figure 4. Raman spectra of fresh GNPs and Rh(0)NCs/GNPs, (a) D + G band, (b) 2D band.

XRD analysis investigated the crystalline property of GNPs before and after Rh-nanocluster decoration. Figure 5 shows the XRD pattern of GNPs and Rh(0)NCs/GNPs catalyst. It can be seen that the XRD pattern of both GNPs and Rh(0)NCs/GNPs show three dominant peaks at $2\theta = 26^\circ$, $2\theta = 44^\circ$, and $2\theta = 55^\circ$ corresponding to (002), (101), and (100) planes of hexagonal graphite structure [31]. However, no new diffraction peaks corresponding to the metallic Rh-nanoclusters were observed for the Rh(0)NCs/GNPs. This is due to the nano-crystalline nature of Rh-nanoclusters and moderately low wt% of Rh in Rh(0)NCs/GNPs (3.65 wt%) [20]. In addition, the fine dispersion of Rh in Rh(0)NCs/GNPs might also be the reason [22].

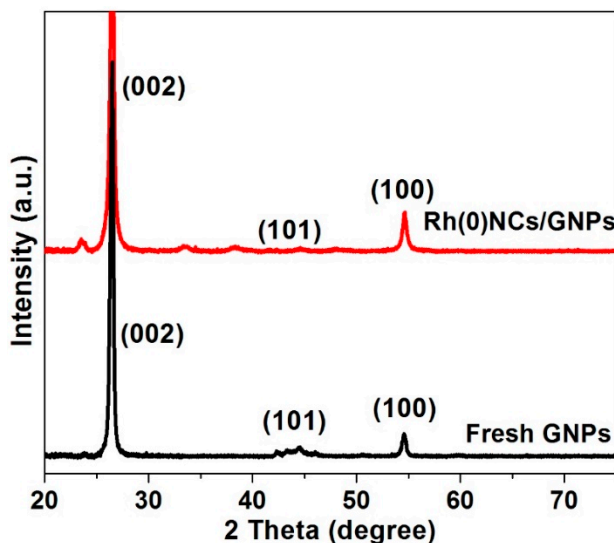


Figure 5. X-ray diffraction (XRD) patterns of fresh GNPs and Rh(0)NCs/GNPs.

The XPS spectra were recorded for the Rh(0)NCs/GNPs and fresh GNPs (Figure 6). It can be noticed that two dominant peaks, C 1s peak at 284.5 eV and O 1s peak at 531.5 eV, were noticed for both GNPs and Rh(0)NCs/GNPs. As expected, the XPS spectrum of Rh(0)NCs/GNPs showed a new peak in the Rh 3d region (Figure 6). The $3d_{3/2}$ peak at 313.2 eV and the Rh $3d_{5/2}$ peak at 307.5 eV confirmed that the Rh-nanoclusters present in the Rh(0)NCs/GNPs are zerovalent Rh [32]. The content of Rh was determined to be 3.51 wt% (agrees well with the EDS data). In addition to the Rh 3d peaks, the presence of O 1s and C 1s peaks clearly shows that the catalyst has oxygen functional groups. The C 1s and O 1s peaks were deconvoluted to find out the oxygen function groups. The deconvolution of C 1s peak resulted in four peaks at 284.1 (C–C/C=C), 284.4 (C–OH), 284.9 (C–O–C), and 287.6 eV (C=O) (Figure 6b) [33]. Similarly, the deconvolution of O 1s peak confirmed the presence of the oxygen function groups, such as C–OH, C–O–C, and C=O (Figure 6c) [34]. It is clear that the oxygen function groups were not completely decomposed during the catalyst preparation process, which might be due to the low calcination temperature (under inert atmosphere at 150 °C for 2 h). We believe that the presence of oxygen functional groups would improve the dispersion of Rh(0)NCs/GNPs catalyst in the aqueous and organic solvents and are therefore suitable for catalytic applications.

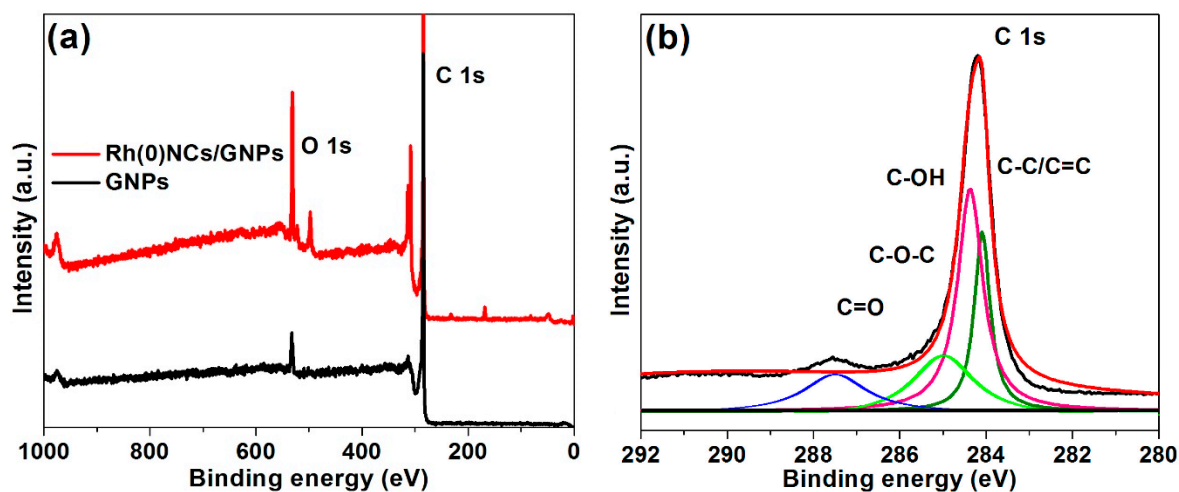


Figure 6. Cont.

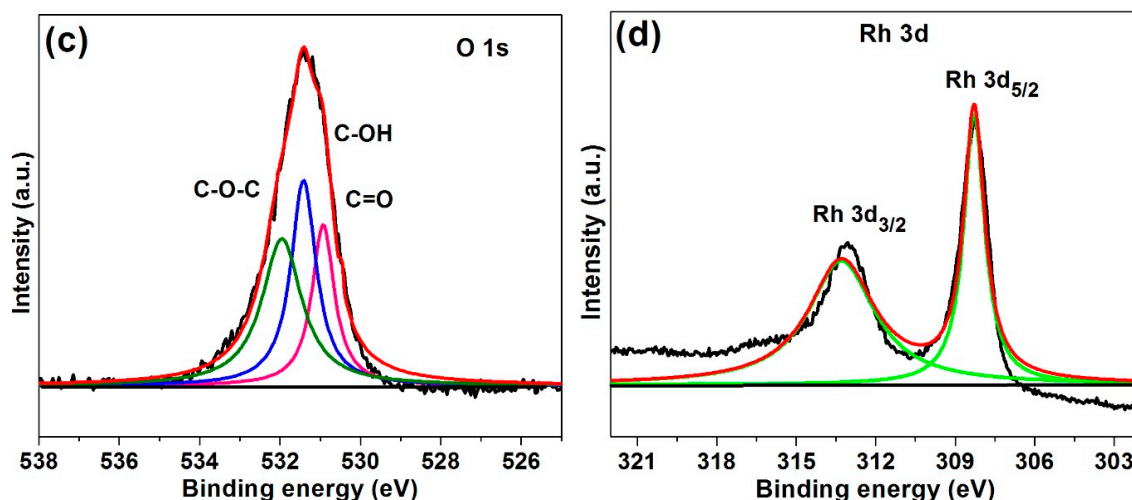


Figure 6. (a) X-ray photoemission spectroscopy (XPS) survey spectrum of Rh(0)NCs/GNPs, and deconvoluted (b) C 1s peak, (c) O 1s peak, and (d) Rh 3d peaks of Rh(0)NCs/GNPs.

2.2. Reduction of 4-Nitrophenol

The catalytic reduction of 4-nitrophenol to 4-aminophenol is one of the significant processes in green chemistry, and the reduction product, 4-aminophenol, is found to be very useful in the preparation of analgesic antipyretic drugs [35,36]. Various mono- and bi-metallic heterogeneous catalysts are reported for the reduction of 4-nitrophenol with NaBH_4 . In particular, metal nanoparticles supported carbon materials (mainly, graphene materials) are found to be the most efficient catalysts for the reduction reaction due to the high surface area and metal-support interaction [37]. In addition, the graphene oxide supported metal catalysts are stable and highly reusable. For instance, Vilian et al. [38] prepared Pdnanospheres decorated reduced graphene oxide catalyst for the removal of hazardous 4-nitrophenol pollutant from water. Similarly, Liu and co-workers [39] reported Ag nanoparticles/graphene-loading loofah sponge hybrid as a catalyst for the conversion of 4-nitrophenol to 4-aminophenol. They found that the catalysts are highly active and reusable. Alike the carbon materials supported catalysts, cellulose nanofibers and mesoporous SBA-15 were also used for the decoration of metal nanoparticles [40,41]. For example, Au, Ag, and Ni nanoparticle immobilized cellulose nanofiber composites were demonstrated to be highly active catalysts in the reduction of 4-nitrophenol [41]. However, the reusability of the catalysts is highly limited. To our delight, the present Rh(0)NCs/GNPs is found to be highly efficient and reusable. The turnover frequency (TOF) value of Rh(0)NCs/GNPs is calculated to be extremely very high (112.5 min^{-1}). Initially, the reaction condition was optimized. The catalytic reactions were monitored by UV-Visible spectroscopy. Figure 7 shows UV-vis spectra of the reduction of 4-nitrophenol while using different amount of Rh(0)NCs/GNPs (0.001, 0.0015, and 0.002 mg). At first, the UV-vis spectra were recorded for the 4-nitrophenol before and after the addition of NaBH_4 . The fresh 4-nitrophenol showed band at 317 nm, whereas the band shifted to 400 nm, after the addition of NaBH_4 . The band at 400 nm confirms the formation of 4-nitrophenolate ion. It was confirmed that the fresh GNPs is not active in the reduction of 4-nitrophenol with NaBH_4 . The UV-vis spectra showed that there is no change in the intensity of 4-nitrophenolate ion peak at 400 nm, even after the stirring for 24 h. Moreover, based on the results, 80 μL of 0.01 M 4-nitrophenol and 4 mL of 0.015 M aqueous NaBH_4 were found to be the optimal amount for performing the reduction reaction. Further, the Rh(0)NCs/GNPs was used for the reduction of 4-nitrophenol (Figure 7). Initially, 1 mg of the catalyst was stirred with a mixture of 80 μL of 0.01 M 4-nitrophenol and 4 mL of 0.015 M aqueous NaBH_4 . Surprisingly, the 4-nitrophenol immediately reduced after the addition of 1 mg of Rh(0)NCs/GNPs, and a new peak corresponding to 4-aminophenol was noticed. Subsequently, the amount of Rh(0)NCs/GNPs was gradually decreased and found that a very low amount of 0.002 mg of catalyst is enough for the complete reduction of 4-nitrophenol to 4-aminophenol. The TOF value

of 112.5 min^{-1} was calculated for the Rh(0)NCs/GNPscatalyzed reduction of 4-nitrophenol. Three different amounts (0.001, 0.0015, and 0.002 mg) of Rh(0)NCs/GNPs was used to study the catalytic reduction reaction. The 0.002 mg of Rh(0)NCs/GNPs just required 2 min for the complete reduction of 4-nitrophenol to 4-aminophenol. Alike, 0.0015 mg of catalyst took about 6 min for the 100% reduction 4-nitrophenol. Figure 7 shows that 0.001 mg of catalyst is not enough for the reduction reaction.

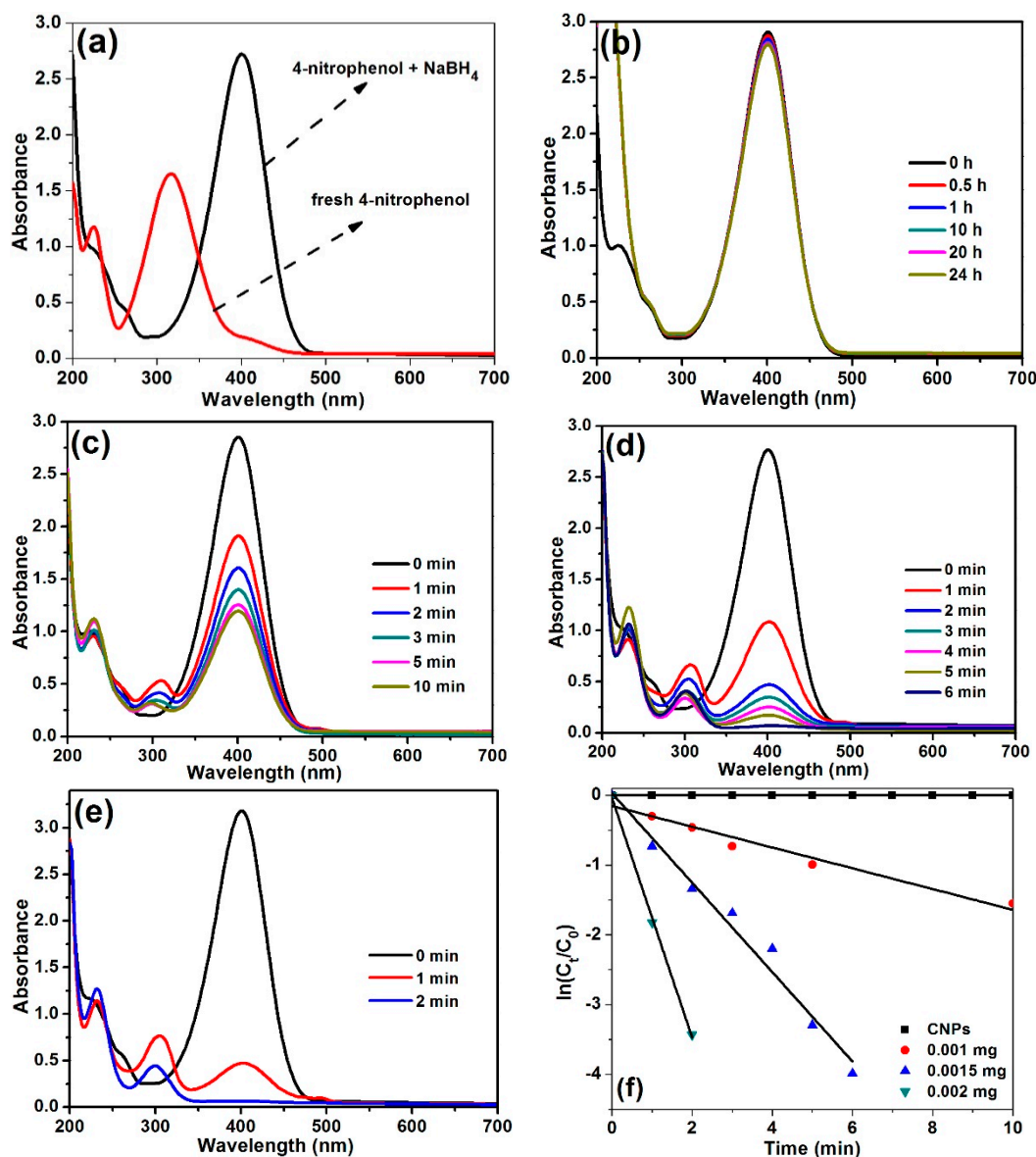


Figure 7. Spectra: (a) 4-nitrophenol before and after addition of NaBH_4 , (b) GNPs catalyzed reduction of 4-nitrophenol with NaBH_4 , (c–e) reduction of 4-nitrophenol using different amount of Rh(0)NCs/GNPs (0.001, 0.0015 and 0.002 mg). (f) Plots of $\ln[C_t/C_0]$ versus reaction time for the reduction of 4-nitrophenol with NaBH_4 over the different amounts of Rh(0)NCs/GNPs.

Figure 7 shows the plots of $\ln[C_t/C_0]$ versus reaction time for the reduction of 4-nitrophenol with NaBH_4 over the different amounts of Rh(0)NCs/GNPs. The linear relationship confirmed that the reduction process follows pseudo-first-order reaction kinetics [39]. The kinetic reaction rate constants (k_{app}) values were obtained from the slope of $\ln(C_t/C_0)$ versus time linear curve. The k_{app} values were calculated to be 14.94 (0.001 mg), 40.05 (0.0015 mg), and $62.07 \times 10^{-3} \text{ min}^{-1}$ (0.002 mg). The values showed that the reduction process is rapid in the presence of the Rh(0)NCs/GNPs. The k' values were also calculated while using the formula: $k' = k_{app}/m$, where m - weight of the metal active site.

Surprisingly, an excellent k' value of 14940, 26700, and $31035 \times 10^{-3} \text{ mg}^{-1} \text{ min}^{-1}$ was obtained for the reduction of 4-nitrophenol, with 0.001, 0.0015, and 0.002 mg of Rh(0)NCs/GNPs, respectively. To the best of our knowledge, this is the best k' values obtained for the reduction of 4-nitrophenol to date.

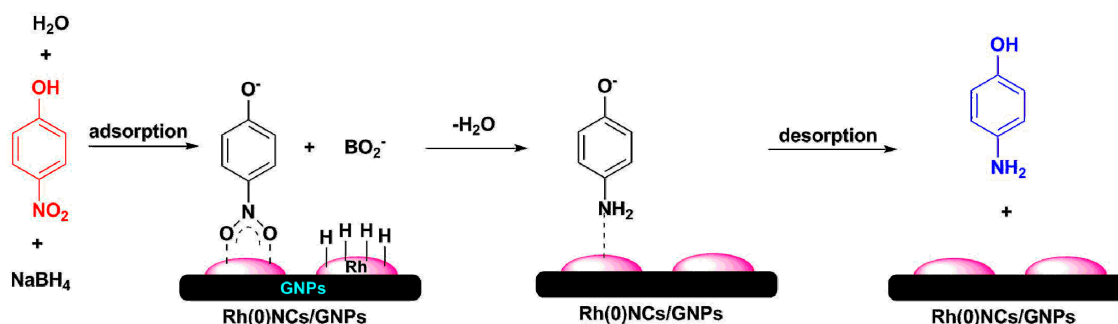
The catalytic activity of Rh(0)NCs/GNPs was compared with previously reported results (Table 1). Wang et al. [42] prepared bimetallic Rh-Ag/r-GO nanocatalyst for the reduction of 4-nitrophenol. The Rh-Ag/r-GO nanocatalyst obtained the highest catalytic with reaction rate of k_{app} value of $14.89 \times 10^{-3} \text{ s}^{-1}$ and k' values of $1415 \text{ s}^{-1} \text{ g}^{-1}$, whereas, the present Rh(0)NCs/GNPs obtained a k_{app} value of $62.07 \times 10^{-3} \text{ min}^{-1}$ and k' values of $31035 \times 10^{-3} \text{ mg}^{-1} \text{ min}^{-1}$. Similarly, the Pt-Au nanodendrites supported on reduced graphene oxide nanosheets catalysts showed a k_{app} value of $3.8 \times 10^{-3} \text{ s}^{-1}$ and k' values of $926 \times 10^{-3} \text{ mg}^{-1} \text{ s}^{-1}$ [43]. Similarly, the catalytic activity of other heterogeneous catalysts, such as Au-Ag/r-GO [44], Ni/MC-750 [45], Ni/GO-2 [21], Ni/GO-1 [21], Pt-Ni/RGO [46], AuNPs-RGO [47], RhAg0.5/rGO [42], RGO-ZnWO₄-Fe₃O₄ [48], AgNPs/RGO-LS [39], Ni/GNP [22], Ru/HHP [49], Ru/C [50], Cu/C [50], and Ni-oxide/GOSs [51] can also be compared to the present catalytic system.

Table 1. Of present Rh(0)NCs/GNPs over other heterogeneous catalysts.

S. No	Catalyst(Amount Used, mg)	Reactant	$k_{\text{app}}(\times 10^{-3} \text{ s}^{-1})$	$k'(\times 10^{-3} \text{ mg}^{-1} \text{ s}^{-1})$	TOF(s^{-1})	References
10	Au-Ag/r-GO (0.1)	4-NP	3.47	34.7	0.042	[42]
7	Ni/MC-750 (3)	4-NP	6.26	20.9	1.44	[43]
4	Ni/GO-2 (0.75)	4-NP	35.4	47.2	25.33	[19]
3	Ni/GO-1 (0.75)	4-NP	28.1	14.0	31.66	[19]
9	Pt-Ni/RGO (3)	4-NP	3.70	1.23	110.9	[44]
12	AuNPs-RGO (0.05)	4-NP	28.37	11.2	0.222	[45]
7	RhAg0.5/rGO	4-NP	14.8	1415	-	[40]
8	Rh(0)NCs/GNPs	4-NP	62.07	31035	112.5	This work
15	RGO-ZnWO ₄ -Fe ₃ O ₄	4-NP	176.8	353.6	-	[46]
10	Ag NPs/RGO-LS	4-NP	32.0	0.4	-	[39]
11	Ni/GNP	4-NP	42.0	2.1	0.38	[22]
12	Ru/HHP	4-NP	62.1	31.1	-	[49]
13	Cu/C	4-NP	0.3	0.13	0.15	[50]
14	Ru/C	4-NP	1.3	0.52	0.29	[50]
15	Ni-oxide/GOSs	4-NP	60.8	60.8	0.73	[51]

TOF, s^{-1} : (turnover frequency) moles of 4-NP converted per mole surface Ni per second.

Based on the results, a mechanism has been proposed for the Rh(0)NCs/GNPs catalyzed reduction of 4-nitrophenol (Scheme 1). The adsorption of 4-nitrophenol molecules on GNPs can be ignored since the fresh GNPs are found to be inactive in the reduction process. At first, the mixing of NaBH₄ and 4-nitrophenol forms 4-nitrophenolate ion. Subsequently, in the next step, the formed 4-nitrophenolate ion adsorbs on the Rh(0)-nanoclusters of Rh(0)NCs/GNPs and an electron transfer from BH₄⁻ to Rh(0)NCs/GNPs produces hydrogen atom on the Rh(0)NCs/GNPs surface with the help of the hydride and the protons (H⁺, provided by H₂O). Finally, the active hydrogen reduces the adsorbed 4-nitrophenolate ion to 4-aminophenol. The 4-aminophenol is desorbed from the Rh(0)NCs/GNPs. The present Rh(0)NCs/GNPs is highly active and it rapidly reduces the 4-nitrophenol with NaBH₄. The rapid reduction of 4-nitrophenol by Rh(0)NCs/GNPs is due to the rapid transfer of electrons from BH₄⁻ to the Rh(0)-nanoclusters with the help of conductive GNPs-support. Surprisingly, highly desirable environmental and economic benefits of Rh(0)NCs/GNPs are realized from its reusability. It was found that the Rh(0)NCs/GNPs can be reused without any significant loss in its catalytic activity. After the fifth cycle, the Rh(0)NCs/GNPs showed over 99% conversion of 4-nitrophenol to 4-aminophenol (Figure 8). The activity of Rh(0)NCs/GNPs was retained for several catalytic runs, but no extra measurements were made for the used catalyst.



Scheme 1. Proposed mechanism for the reduction 4-nitrophenol to 4-aminophenol by Rh(0)NCs/GNPs.

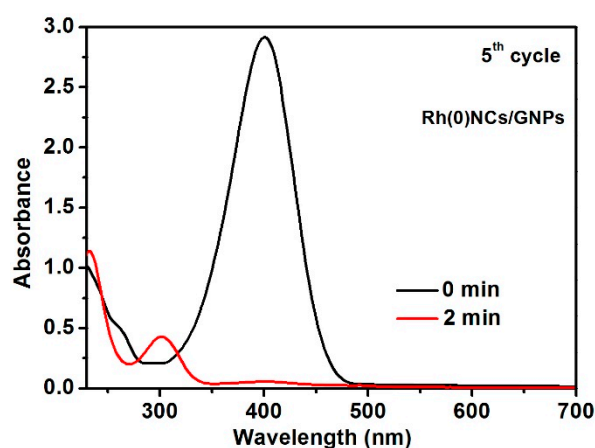
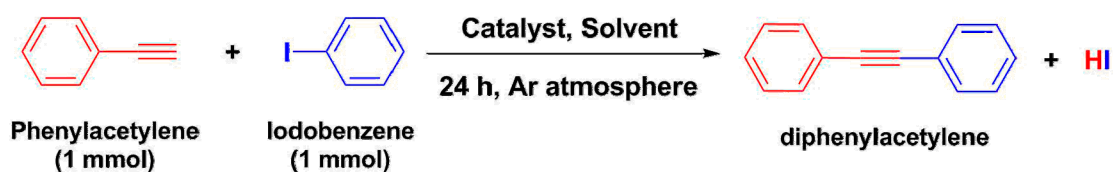


Figure 8. Spectra of the reduction of 4-nitrophenol using 0.002 mg of used Rh(0)NCs/GNPs (5th cycle).

2.3. Sonogashira Coupling Reaction

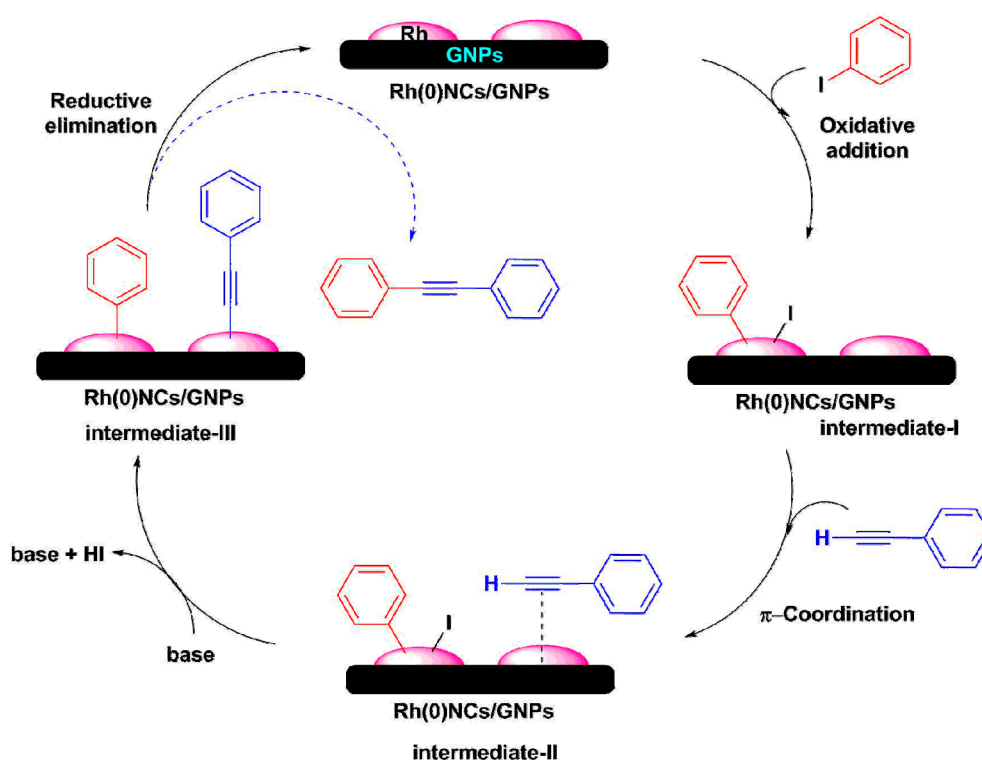
Transition metal catalyzed C–C bond forming reactions are significant tools in organic synthesis. Catalytic products that are prepared via Sonogashira coupling reaction between terminal alkynes and aryl halides have significant value in pharmaceuticals and fine chemicals [52]. To date, several transition metal based heterogeneous catalysts are developed for the Sonogashira coupling reaction [53]. However, most of them are bimetallic catalysts and its preparation method requires toxic reagents. For instance, the Pd–Cu bimetallic system was developed for the cross-coupling of terminal acetylenes with sp²-carbon halides by Sonogashira [54]. Similarly, monodisperse CuPd alloy nanoparticles supported graphene oxide catalyst was prepared for the Sonogashira coupling reaction [55]. They found that the bimetallic catalyst is very active and selective. Later, affordable mono metallic catalysts based on Pd, Ni, Cu, Fe, and Co were developed for a more sustainable cross-coupling catalysis [56,57]. After being characterized, the Rh(0)NCs/GNPs was used as catalyst for the Sonogashira coupling reaction of iodobenzene with phenylacetylene (Scheme 2). To our delight, the present Rh(0)NCs/GNPs showed good catalytic activity towards the cross-coupling reaction. The reaction condition was optimized. A 20 mg of Rh(0)NCs/GNPs, tetra butyl ammonium acetate (1 mmol) and 10 mL of DMF were found to be optimal parameters for performing the cross-coupling of iodobenzene with phenylacetylene. The optimal reaction temperature and reaction time were found to be 120 °C and 24 h, respectively. Under the optimal conditions, the Rh(0)NCs/GNPs gave the desired product, diphenylacetylene, in a good yield of 87% with 91% selectivity. Kanuru et al. [26] reported 5 wt% of Rh nanoparticles supported γ -Alumina catalyst (Rh/ γ -Al₂O₃) for the cross-coupling iodobenzene with phenylacetylene. The Rh/ γ -Al₂O₃ catalyst showed just 57% of the targeted product diphenylacetylene. Similarly, the Rh/BaO catalyst affords 38% of the product. It might be due to the good interaction between Rh-nanoparticles and GNPs, high surface area, optimal size of Rh-nanoparticles, and fine dispersion of catalyst. A reusability test was also performed for the Rh(0)NCs/GNPs. The catalyst gave good 77% yield even after the fifth cycle. The reaction mixture was centrifuged to remove the catalyst

and the mixture was tested by ICP-MS in order to check the leaching of Rh(0) from the Rh(0)NCs/GNPs. It was found that there is no significant leaching of Rh during the reaction (leaching amount of Rh was 1.3 ppm).



Scheme 2. Sonogashira coupling reaction of iodobenzene with phenylacetylene in the presence of base and solvent catalyzed by Rh(0)NCs/GNPs.

Scheme 3 shows the proposed mechanism for the Rh(0)NCs/GNPs catalyzed Sonogashira cross-coupling of iodobenzene with phenylacetylene. At first, the iodobenzene adsorbs on the Rh(0)NCs/GNPs surface through oxidative addition and it forms intermediate-I. Subsequently, π -coordination takes place between phenylacetylene and intermediate-I to form intermediate-II. Next, the intermediate-II undergoes deprotonation with the help of base and it forms intermediate-III. Finally, the intermediate-III undergoes reductive elimination and gives the catalytic product, diphenylacetylene.



Scheme 3. Plausible mechanism for Rh(0)NCs/GNPs catalyzed Sonogashira cross-coupling of iodobenzene with phenylacetylene.

Overall, the present Rh(0)NCs/GNPs found to be active catalyst for the reduction of 4-nitrophenol and the Sonogashira coupling reaction. In fact, high surface area, good interaction between Rh(0)-nanocluster and GNPs, and the small size of Rh(0)-nanocluster are the main reasons for the good catalytic performance of Rh(0)NCs/GNPs. In addition, the creation of additional defect sites in GNPs by mechanical girding during the catalyst preparation process is also the reason.

3. Experimental Section

3.1. Materials

Rh-acetylacetonate ($\text{Rh}(\text{acac})_3$), 4-nitrophenol, phenylacetylene, iodobenzene, sodium borohydride (NaBH_4), base, and solvents were purchased from Sigma Aldrich, Saint Louis, MO, USA. Nano-scaled graphene platelets were received from ACS materials, Pasadena, CA, USA. All other chemicals used as received.

3.2. Preparation of Rh(0)NCs/GNPs

The preparation method includes no reducing or capping agents to control the morphology of Rh(0)NCs/GNPs. At first, a mixture of 500 mg of GNPs, 100 mg of $\text{Rh}(\text{acac})_3$, and 25 mL of distilled water was sonicated at 60 °C for 20 min followed by stirring at 100 °C for 3 h. Then the reaction mixture was heated at 110 °C in order to evaporate the water and solid mixture of GNPs/ $\text{Rh}(\text{acac})_3$ was obtained. Subsequently, the obtained solid mixture was grinded using mortar and pestle for 15 min to obtain homogenous mixture of GNPs/ $\text{Rh}(\text{acac})_3$. Finally, the resultant homogenous mixture was calcinated under inert atmosphere at 150 °C for 2 h to obtain the Rh(0)NCs/GNPs catalyst.

3.3. Characterization

The morphology of Rh(0)NCs/GNPs catalyst was studied by TEM analysis (TEM, JEOL JEM-2100F). The accelerating voltage of 200 kV was set to record the TEM images. The SEM image and EDS spectrum (Hitachi 3000H SEM) were recorded to determine the Rh-content in Rh(0)NCs/GNPs. XRD (Rigaku Ultima XRD) and Raman spectroscopy (LabRam ARAMIS IR2) are used to study crystalline nature and metal-support interaction of fresh GNPs and Rh(0)NCs/GNPs. XPS was recorded on Kratos Axis-Ultra DLD, Kratos Analytical Ltd., Kanagawa, Japan. UV-vis (Shimadzu UV-2600 spectrophotometer) spectra were recorded to study the catalytic activity of Rh(0)NCs/GNPs towards the reduction of 4-nitrophenol. GC (Shimadzu-2010 gas chromatograph, Kyoto, Japan) and NMR (400 MHz Bruker spectrometer, Ettlingen, Germany) were used to confirm the catalytic products.

3.4. Procedure for Sonogashira Coupling Reaction

A mixture of iodobenzene (1 mmol, 204 mg), phenylacetylene (1 mmol, 102 mg), base (1 mmol), DMF (10 mL), and Rh(0)NCs/GNPs (5 mg) was stirred under argon atmosphere at 120 °C for 24 h. Carousel reactor station (Radleys, Essex, Saffron Walden CB11 3AZ, United Kingdom) was used to carry out the reaction. After 24 h of stirring, the reaction mixture was centrifuged to remove the catalyst, and GC and NMR were then used to analyze the mixture. The recovered catalyst was used to test the reusability. GC determined the yield and selectivity of the catalytic products. Diphenylacetylene: ^1H NMR (400 MHz, CDCl_3): δ 7.58–7.61 (m, 2H), 7.45–7.49 (m, 1H), 7.41–7.45 (m, 2H). ^{13}C NMR (CDCl_3): δ 133.1, 132.3, 121.5, 129.2, 82.3.

3.5. Procedure for 4-Nitrophenol Reduction

In a typical procedure, a mixture of aqueous solution of 4-nitrophenol (80 μL , 0.01 M), aqueous solution of NaBH_4 (4 mL, 0.015 M) and Rh(0)NCs/GNPs (0.001 mg, 0.0015, or 0.002 mg) was initially sonicated for 15 s, followed by stirring under open air atmosphere at 27 °C. UV-vis spectroscopy was operated at room temperature to monitor the reaction at regular time intervals. The catalyst was recovered for reusability test after completion of the reaction.

4. Conclusions

In summary, highly efficient Rh(0)-nanoclusters supported graphene nano-platelets catalyst was prepared by a very simple 'mix and heat' method. The surface morphology, crystalline properties, and chemical state of the resultant Rh(0)NCs/GNPs were investigated by means of

various microscopic and spectroscopic techniques. Raman was used to study the interaction between Rh(0)-nanoclusters and GNPs. The factual Rh-loading in Rh(0)NCs/GNPs was confirmed by SEM-EDS and ICP-MS analysis. After being characterized, the Rh(0)NCs/GNPs was used as nanocatalyst for the reduction of 4-nitrophenol and Sonogashira coupling reactions. The Rh(0)NCs/GNPs demonstrated excellent catalytic activity in the reduction of 4-nitrophenol. The k_{app} , k' and TOF values were calculated to be $62.07 \times 10^{-3} \text{ min}^{-1}$ (0.002 mg of Rh(0)NCs/GNPs), $31035 \times 10^{-3} \text{ mg}^{-1} \text{ min}^{-1}$ and 112.5 min^{-1} , respectively. Similarly, under the optimal conditions, the Rh(0)NCs/GNPs gave the desired product, diphenylacetylene, in a good yield of 87% with 91% selectivity. The Rh(0)NCs/GNPs can be reused without significant loss in its catalytic activity. To the best our knowledge, this is the most efficient, stable, and reusable Rh-based graphene catalyst for the reduction of 4-nitrophenol and Sonogashira coupling reaction reported to date.

Author Contributions: Conceptualization and methodology, G.M., K.I.S., and C.I.M.; Formal analysis, G.M., and S.S.; Software and formal analysis, S.U., and G.M.; Data curation and investigation, G.M. and S.S.; Original draft writing and review and editing, G.M., C.I.M. and K.I.S.; Supervision, I.A., C.I.M. and K.I.S.

Funding: This research received no external funding.

Acknowledgments: This study was supported by Konkuk University KU research professor program.

Conflicts of Interest: The authors declare no conflict of interest.

References

1. Dhiman, M.; Chalke, B.; Polshettiwar, V. Efficient Synthesis of Monodisperse Metal (Rh, Ru, Pd) Nanoparticles Supported on Fibrous Nanosilica (KCC-1) for Catalysis. *ACS Sustain. Chem. Eng.* **2015**, *3*, 3224–3230. [[CrossRef](#)]
2. Jia, C.J.; Schuth, F. Colloidal Metal Nanoparticles as a Component of Designed Catalyst. *Phys. Chem. Chem. Phys.* **2011**, *13*, 2457–2487. [[CrossRef](#)] [[PubMed](#)]
3. Sharma, S.; Bhattacharjee, D.; Das, P. Supported Rhodium Nanoparticles Catalyzed Reduction of Nitroarenes, Arylcarbonyls and Aryl/Benzyl Sulfoxides using Ethanol/Methanol as In Situ Hydrogen Source. *Adv. Synth. Catal.* **2018**, *360*, 2131–2137. [[CrossRef](#)]
4. Jiang, B.; Li, C.; Dag, O.; Abe, H.; Takei, T.; Imai, T.; Hossain, M.S.A.; Islam, M.T.; Wood, K.; Henzie, J.; et al. Mesoporous Metallic Rhodium Nanoparticles. *Nat. Commun.* **2017**, *8*, 15581. [[CrossRef](#)]
5. Xie, S.; Liu, X.Y.; Xia, Y. Shape-controlled Syntheses of Rhodium Nanocrystals for the Enhancement of their Catalytic Properties. *Nano Res.* **2015**, *8*, 82–96. [[CrossRef](#)]
6. Zhang, X.; Li, P.; Barreda, A.; Gutierrez, Y.; Gonzalez, F.; Moreno, F.; Everitt, H.O.; Liu, J. Size-Tunable Rhodium Nanostructures for Wavelength-Tunable Ultraviolet Plasmonics. *Nanoscale Horiz* **2016**, *1*, 75–80. [[CrossRef](#)]
7. Kang, S.; Shin, W.; Choi, M.H.; Ahn, M.; Kim, Y.K.; Kim, S.; Min, D.H.; Jang, H. Morphology-Controlled Synthesis of Rhodium Nanoparticles for Cancer Phototherapy. *ACS Nano* **2018**, *12*, 6997–7008. [[CrossRef](#)]
8. Siebels, M.; Schlusener, C.; Thomas, J.; Xiao, Y.X.; Yang, X.Y.; Janiak, C. Rhodium Nanoparticles Supported on Covalent Triazine-based Frameworks as Reusable Catalyst for Benzene Hydrogenation and Hydrogen Evolution Reaction. *J. Mater. Chem. A* **2019**, *7*, 11934–11943. [[CrossRef](#)]
9. Motoyama, Y.; Takasaki, M.; Yoon, S.H.; Mochida, I.; Nagashima, H. Rhodium Nanoparticles Supported on Carbon Nanofibers as an Arene Hydrogenation Catalyst Highly Tolerant to a Coexisting Epoxido Group. *Org. Lett.* **2009**, *11*, 5042–5045. [[CrossRef](#)]
10. Huang, C.; Li, C.; Shi, G. Graphene Based Catalysts. *Energy Environ. Sci.* **2012**, *5*, 8848–8868. [[CrossRef](#)]
11. Gopiraman, M.; Chung, I.M. Highly Active and Cost-effective CuO-based Carbon Nanocomposite with Unique Morphology for Catalytic Synthesis of Imines under Solvent-free Conditions. *J. Taiwan. Inst. Chem. Eng.* **2017**, *81*, 455–464. [[CrossRef](#)]
12. Qiao, F.; Yang, J.; Liang, Q.; Wang, X.; Xu, Q.; Wang, Q. Fabrication of 3D Graphene/CdTe Quantum Dots Composite through Electrophoretic Deposition and its Electrical Properties. *J. Mater. Sci. Mater. Electron.* **2017**, *28*, 15333–15337. [[CrossRef](#)]

13. Zeng, M.; Shah, S.A.; Huang, D.; Parviz, D.; Yu, Y.H.; Wang, X.; Green, M.J.; Cheng, Z. Aqueous Exfoliation of Graphite into Graphene Assisted by SulfonylGraphene Quantum Dots for Photonic Crystal Applications. *ACS Appl. Mater. Interfaces* **2017**, *9*, 30797–30804. [[CrossRef](#)] [[PubMed](#)]
14. Cheng, Y.; Fan, Y.; Pei, Y.; Qiao, M. Graphene-supported Metal/metal Oxide Nanohybrids: Synthesis and Applications in Heterogeneous Catalysis. *Catal. Sci. Technol.* **2015**, *5*, 3903–3916. [[CrossRef](#)]
15. Lin, Y.; Watson, K.A.; Fallbach, M.J.; Ghose, S.; Smith, J.G., Jr.; Delozier, D.M.; Cao, W.; Crooks, R.E.; Connell, J.W. Rapid, Solventless, Bulk Preparation of Metal Nanoparticle-Decorated Carbon Nanotubes. *ACS Nano* **2009**, *3*, 871–884. [[CrossRef](#)]
16. Gopiraman, M.; Karvembu, R.; Kim, I.S. Highly Active, Selective, and Reusable RuO₂/SWCNT Catalyst for Heck Olefination of Aryl Halides. *ACS Catal.* **2014**, *4*, 2118–2129. [[CrossRef](#)]
17. Gopiraman, M.; Deng, D.; Ganesh Babu, S.; Hayashi, T.; Karvembu, R.; Kim, I.S. Sustainable and Versatile CuO/GNS Nanocatalyst for Highly Efficient Base Free Coupling Reactions. *ACS Sustain. Chem. Eng.* **2015**, *3*, 2478–2488. [[CrossRef](#)]
18. Gopiraman, M.; Babu, S.G.; Karvembu, R.; Kim, I.S. Nanostructured RuO₂ on MWCNTs: Efficient Catalyst for Transfer Hydrogenation of Carbonyl Compounds and Aerial Oxidation of Alcohols. *Appl. Catal. A* **2014**, *484*, 84–96. [[CrossRef](#)]
19. Gopiraman, M.; Babu, S.G.; Khatri, Z.; Kai, W.; Kim, Y.A.; Endo, M.; Karvembu, R.; Kim, I.S. An Efficient, Reusable Copper-oxide/carbon-nanotube Catalyst for N-Arylation of Imidazole. *Carbon* **2013**, *62*, 135–148. [[CrossRef](#)]
20. Gopiraman, M.; Ganesh Babu, S.; Khatri, Z.; Kai, W.; Kim, Y.A.; Endo, M.; Kim, I.S. Dry Synthesis of Easily Tunable Nano Ruthenium Supported on Graphene: Novel Nanocatalysts for Aerial Oxidation of Alcohols and Transfer Hydrogenation of Ketones. *J. Phys. Chem. C* **2013**, *117*, 23582–23596. [[CrossRef](#)]
21. Gopiraman, M.; Saravanamoorthy, S.; Deng, D.; Ilangoan, A.; Kim, I.S.; Chung, I.M. Facile Mechanochemical Synthesis of Nickel/Graphene Oxide Nanocomposites with Unique and Tunable Morphology: Applications in Heterogeneous Catalysis and Supercapacitors. *Catalysts* **2019**, *9*, 486. [[CrossRef](#)]
22. Somasundaram, S.; Ill-Min, C.; Vanaraj, R.; Ramagathan, B.; Mayakrishnan, G. Highly Active and Reducing Agent-free Preparation of Cost-effective NiO-based Carbon Nanocomposite and its Application in Reduction Reactions under Mild Conditions. *J. Ind. Eng. Chem.* **2018**, *60*, 91–101. [[CrossRef](#)]
23. Gopiraman, M.; Bang, H.; Babu, S.G.; Wei, K.; Karvembu, R.; Kim, I.S. Catalytic N-oxidation of Tertiary Amines on RuO₂ NPs Anchored Graphene Nanoplatelets. *Catal. Sci. Technol.* **2014**, *4*, 2099–2106. [[CrossRef](#)]
24. Zhao, P.; Feng, X.; Huang, D.; Yang, G.; Astruc, D. Basic Concepts and Recent Advances in Nitrophenol Reduction by Gold-and other Transition Metal Nanoparticles. *Coord. Chem. Rev.* **2015**, *287*, 114–136. [[CrossRef](#)]
25. Liori, A.A.; Stamatopoulos, I.K.; Papastavrou, A.T.; Pinaka, A.; Vougioukalakis, G.C. A Sustainable, User-Friendly Protocol for the Pd-Free Sonogashira Coupling Reaction. *Eur. J. Org. Chem.* **2018**, *2018*, 6134–6139. [[CrossRef](#)]
26. Kanuru, V.K.; Humphrey, S.M.; Kyffin, J.M.; Jefferson, D.A.; Burton, J.W.; Armbruster, M.; Lambert, R.M. Evidence for Heterogeneous Sonogashira Coupling of Phenylacetylene and Iodobenzene Catalyzed by Well Defined Rhodium Nanoparticles. *Dalton Trans.* **2009**, *37*, 7602–7605. [[CrossRef](#)] [[PubMed](#)]
27. Yuan, Y.; Yan, N.; Dyson, P.J. Advances in the Rational Design of Rhodium Nanoparticle Catalysts: Control via Manipulation of the Nanoparticle Core and Stabilizer. *ACS Catal.* **2012**, *2*, 1057–1069. [[CrossRef](#)]
28. Khan, M.E.; Khan, M.M.; Cho, M.H. Defected Graphene Nano-platelets for Enhanced Hydrophilic Nature and Visible Light-induced Photoelectrochemical Performances. *J. Phys. Chem. Solids* **2017**, *104*, 233–242. [[CrossRef](#)]
29. Sujith, R.; Chauhan, P.K.; Gangadhar, J.; Maheshwari, A. Graphene Nanoplatelets as Nanofillers in Mesoporous Silicon Oxycarbide Polymer Derived Ceramics. *Sci. Rep.* **2018**, *8*, 17633. [[CrossRef](#)]
30. Sheng, Z.H.; Shao, L.; Chen, J.J.; Bao, W.J.; Wang, F.B.; Xia, X.H. Catalyst-free Synthesis of Nitrogen-doped Graphene via Thermal Annealing Graphite Oxide with Melamine and its Excellent Electrocatalysis. *ACS Nano* **2011**, *5*, 4350–4358. [[CrossRef](#)]
31. Dong, L.; Yu, W.; Liu, M.; Liu, Y.; Shao, Q.; Li, A.; Yan, W. Novel Composite Electrode of the Reduced Graphene Oxide Nanosheets with Gold Nanoparticles Modified by Glucose Oxidase for Electrochemical Reactions. *Catalysts* **2019**, *9*, 764. [[CrossRef](#)]

32. Jin, C.; Xia, W.; Nagaiah, T.C.; Guo, J.; Chen, X.; Bron, M.; Schuhmann, W.; Muhler, M. On the Role of the Thermal Treatment of Sulfided Rh/CNT Catalysts Applied in the Oxygen Reduction Reaction. *Electrochim. Acta* **2009**, *54*, 7186–7193. [[CrossRef](#)]
33. Nancy, P.; Nair, A.K.; Antoine, R.; Thomas, S.; Kalarikkal, N. In Situ Decoration of Gold Nanoparticles on Graphene Oxide via Nanosecond Laser Ablation for Remarkable Chemical Sensing and Catalysis. *Nanomaterials* **2019**, *9*, 1201. [[CrossRef](#)] [[PubMed](#)]
34. Abdolhosseinzadeh, S.; Asgharzadeh, H.; Kim, H.S. Fast and Fully-scalable Synthesis of Reduced Graphene Oxide. *Sci. Rep.* **2015**, *5*, 10160. [[CrossRef](#)] [[PubMed](#)]
35. Shah, K.W.; Zheng, L. Microwave-assisted Synthesis of Hexagonal Gold Nanoparticles Reduced by Organosilane (3-Mercaptopropyl) trimethoxysilane. *Materials* **2019**, *12*, 1680. [[CrossRef](#)]
36. Sun, L.; Xiang, X.; Wu, J.; Cai, C.; Ao, D.; Luo, J.; Tian, C.; Zu, X. Bi-Metal Phosphide NiCoP: An Enhanced Catalyst for the Reduction of 4-Nitrophenol. *Nanomaterials* **2019**, *9*, 112. [[CrossRef](#)]
37. Morales, M.V.; Rocha, M.; Freire, C.; Asedegbega-Nieto, E.; Gallegos-Suarez, E.; Rodríguez-Ramos, I.; Guerrero-Ruiz, A. Development of Highly Efficient Cu versus Pd Catalysts Supported on Graphitic Carbon Materials for the Reduction of 4-Nitrophenol to 4-Aminophenol at Room Temperature. *Carbon* **2017**, *111*, 150–161. [[CrossRef](#)]
38. Vilian, A.E.; Choe, S.R.; Giribabu, K.; Jang, S.C.; Roh, C.; Huh, Y.S.; Han, Y.K. PdNanospheres Decorated Reduced Graphene Oxide with Multi-functions: Highly Efficient Catalytic Reduction and Ultrasensitive Sensing of Hazardous 4-Nitrophenol Pollutant. *J. Hazard. Mater.* **2017**, *333*, 54–62. [[CrossRef](#)]
39. Liu, Y.Y.; Zhao, Y.H.; Zhou, Y.; Guo, X.L.; Chen, Z.T.; Zhang, W.J.; Zhang, Y.; Chen, J.; Wang, Z.M.; Sun, L.T.; et al. High-efficient Catalytic Reduction of 4-Nitrophenol based on Reusable Ag Nanoparticles/graphene-loading Loofah Sponge Hybrid. *Nanotechnology* **2018**, *29*, 315702. [[CrossRef](#)]
40. Sareen, S.; Mutreja, V.; Pal, B.; Singh, S. Synthesis of Bimetallic Au-Ag Alloyed Mesocomposites and their Catalytic Activity for the Reduction of Nitroaromatics. *Appl. Surf. Sci.* **2018**, *435*, 552–562. [[CrossRef](#)]
41. Gopiraman, M.; Deng, D.; Saravanamoorthy, S.; Chung, I.M.; Kim, I.S. Gold, Silver and Nickel Nanoparticle Anchored Cellulose Nanofiber Composites as Highly Active Catalysts for the Rapid and Selective Reduction of Nitrophenols in Water. *RSC Adv.* **2018**, *8*, 3014–3023. [[CrossRef](#)]
42. Wang, C.; Ciganda, R.; Yate, L.; Moya, S.; Salmon, L.; Ruiz, J.; Astruc, D. RhAg/rGONanocatalyst: Ligand-controlled Synthesis and Superior Catalytic Performances for the Reduction of 4-Nitrophenol. *J. Mater. Sci.* **2017**, *52*, 9465–9476. [[CrossRef](#)]
43. Lv, J.J.; Wang, A.J.; Ma, X.; Xiang, R.Y.; Chen, J.R.; Feng, J.J. One-pot synthesis of porous Pt–Au nanodendrites supported on reduced graphene oxide nanosheets toward catalytic reduction of 4-nitrophenol. *J. Mater. Chem. A* **2015**, *3*, 290–296. [[CrossRef](#)]
44. Hareesh, K.; Joshi, R.P.; Sunitha, D.V.; Bhoraskar, V.N.; Dhole, S.D. Anchoring of Ag-Au Alloy Nanoparticles on Reduced Graphene Oxide Sheets for the Reduction of 4-Nitrophenol. *Appl. Surf. Sci.* **2016**, *389*, 1050–1055.
45. Yang, Y.; Ren, Y.; Sun, C.; Hao, S. Facile Route Fabrication of Nickel based Mesoporous Carbons with High Catalytic Performance towards 4-Nitrophenol Reduction. *Green Chem.* **2014**, *16*, 2273–2280. [[CrossRef](#)]
46. Zhao, F.; Kong, W.; Hu, Z.; Liu, J.; Zhao, Y.; Zhang, B. Tuning the Performance of Pt–Ni Alloy/reduced Graphene Oxide Catalysts for 4-Nitrophenol Reduction. *RSC Adv.* **2016**, *6*, 79028–79036. [[CrossRef](#)]
47. Vellaichamy, B.; Periakaruppan, P.; Thomas, J. Synthesis of AuNPs@RGONanosheets for Sustainable Catalysis toward Nitrophenols Reduction. *Ultrason. Sonochem.* **2018**, *48*, 362–369. [[CrossRef](#)]
48. Mohamed, M.J.S.; Denthaje, K.B. Novel RGO-ZnWO₄-Fe₃O₄Nanocomposite as an Efficient Catalyst for Rapid Reduction of 4-Nitrophenol to 4-Aminophenol. *Ind. Eng. Chem. Res.* **2016**, *55*, 7267–7272. [[CrossRef](#)]
49. Gopiraman, M.; Saravanamoorthy, S.; Chung, I.M. Highly Active Human-hair-supported Noble Metal (Ag or Ru) Nanocomposites for Rapid and Selective Reduction of p-Nitrophenol to p-Aminophenol. *Res. Chem. Intermed.* **2017**, *43*, 5601–5614. [[CrossRef](#)]
50. Gopiraman, M.; Muneeswaran, M.; Kim, I.S. Highly Porous Ru/C and Cu/C Nanocatalysts derived from Custard Apple for Rapid and Selective Reduction of p-Nitrophenol. *Nano Prog.* **2019**, *1*, 30–36. [[CrossRef](#)]
51. Saravanamoorthy, S.; Vijayakumar, E.; Jemimah, S.; Ilangovan, A. Catalytic Reduction of p-Nitrophenol and Carbonyl Compounds by NiO-nanoparticles Fastened Graphene Oxide. *Chem. Sci. Eng. Res.* **2019**, *1*, 1–7.
52. Chinchilla, R.; Najera, C. Recent Advances in Sonogashira Reactions. *Chem. Soc. Rev.* **2011**, *40*, 5084–5121. [[CrossRef](#)] [[PubMed](#)]

53. Karami, K.; Abedanzadeh, S.; Hervés, P. Synthesis and Characterization of Functionalized Titania-supported Pd Catalyst deriving from New Orthopalladated Complex of Benzophenone Imine: Catalytic Activity in the Copper-free Sonogashira Cross-Coupling Reactions at Low Palladium Loadings. *RSC Adv.* **2016**, *6*, 93660–93672. [[CrossRef](#)]
54. Sonogashira, K. Development of Pd–Cu Catalyzed Cross-Coupling of Terminal Acetylenes with sp^2 -carbon Halides. *J. Organomet. Chem.* **2002**, *653*, 46–49. [[CrossRef](#)]
55. Diyarbakir, S.; Can, H.; Metin, O. Reduced Graphene Oxide-supported CuPd Alloy Nanoparticles as Efficient Catalysts for the Sonogashira Cross-coupling Reactions. *ACS Appl. Mater. Interfaces* **2015**, *7*, 3199–3206. [[CrossRef](#)] [[PubMed](#)]
56. Ikeda, Y.; Nakamura, T.; Yorimitsu, H.; Oshima, K. Cobalt-catalyzed Heck-type Reaction of Alkyl Halides with Styrenes. *J. Am. Chem. Soc.* **2002**, *124*, 6514–6515. [[CrossRef](#)]
57. Firouzabadi, H.; Iranpoor, N.; Gholinejad, M.; Hoseini, J. Magnetite (Fe_3O_4) Nanoparticles-catalyzed Sonogashira–Hagihara Reactions in Ethylene Glycol under Ligand-free Conditions. *Adv. Synth. Catal.* **2011**, *353*, 125–132. [[CrossRef](#)]



© 2019 by the authors. Licensee MDPI, Basel, Switzerland. This article is an open access article distributed under the terms and conditions of the Creative Commons Attribution (CC BY) license (<http://creativecommons.org/licenses/by/4.0/>).